Journal of Materials Chemistry C

Sn(SCN)2 as an Additive for Improving Hole Transport Properties of PEDOT:PSS in Organic Photovoltaics

Journal:	*Journal of Materials Chemistry C*
Manuscript ID	TC-ART-06-2023-002075.R1
Article Type:	Paper
Date Submitted by the Author:	22-Aug-2023
Complete List of Authors:	Chaopaknam, Jidapa; Vidyasirimedhi Institute of Science and Technology (VISTEC), School of Molecular Science and Engineering, Department of Materials Science and Engineering Sudyoadsuk, Taweesak; Vidyasirimedhi Institute of Science and Technology Promarak, Vinich; Vidyasirimedhi Institute of Science and Technology, Molecular Science and Engineering Saeki, Akinori; Osaka University, Department of Applied Chemistry, Graduate School of Engineering Pattanasattayavong, Pichaya; Vidyasirimedhi Institute of Science and Technology (VISTEC), Department of Materials Science and Engineering

$Sn(SCN)_2$ as an Additive for Improving Hole Transport Properties of PEDOT:PSS in Organic Photovoltaics

Jidapa Chaopaknam,[ab] Taweesak Sudyoadsuk,[a] Vinich Promarak,[a] Akinori Saeki,[b] and Pichaya Pattanasattayavong*[a]

[a] Department of Materials Science and Engineering, School of Molecular Science and Engineering, Vidyasirimedhi Institute of Science and Technology (VISTEC), Rayong 21210, Thailand

[b] Department of Applied Chemistry, Graduate School of Engineering, Osaka University, 2-1 Yamadaoka, Suita, Osaka 565-0871, Japan

* Corresponding author. Email: pichaya.p@vistec.ac.th

Abstract

Tin(II) thiocyanate [$Sn(SCN)_2$] has been recently demonstrated as an anode interlayer and additive in the electron transport layer (ETL) for organic photovoltaics (OPVs). We further demonstrate herein the application of this emerging electronic material as an additive for poly(3,4-ehtylenedioxythiophene)-poly(styrene-sulfonate) (PEDOT:PSS), employed as a hole transport layer (HTL) in OPVs. $Sn(SCN)_2$ is processable using common solvents; the addition of a small amount of $Sn(SCN)_2$ leads to some removal of PSS and dedopes PEDOT. Despite the lower conductivity, the simple process effectively enhances the hole transport properties and overall device performance. The optimal additive concentration yields an increase in the average power conversion efficiency (PCE) from 9.0% (pristine) to 9.8% [$Sn(SCN)_2$-added] for OPVs based on a well-known bulk-heterojunction layer.

Keywords: tin(II) thiocyanate, PEDOT, dedoping, hole transport layers, organic photovoltaics

1. Introduction

The recent advancements in organic photovoltaics (OPVs) have invigorated the research field as the power conversion efficiency (PCE) of single-junction cells is surpassing 18% and expected to reach 20%.[1–5] In the modern OPV cell structure, interlayer materials also play an important part, particularly for optimizing charge extraction and minimizing charge recombination.[6,7] Historically, poly(3,4-ethylene dioxythiophene):poly (styrenesulfonate) (PEDOT: PSS) has been a longstanding choice as a hole-transport layer (HTL), an interlayer between the anode and the photoactive layer, due to its relatively high p-type conductivity, along with high transparency (80-87% in the visible spectrum), large work function (≈5.1 eV), and good film-forming properties from solution-based depositions.[8–10]

PEDOT:PSS is a polyelectrolyte comprising the positively charged PEDOT chains and the negatively charged PSS chains. Although PSS dopes (oxidizes) PEDOT to generate the positive charge carriers, by itself PSS is insulating and can impede the conductivity in the film.[11] Nevertheless, an excess amount of PSS is crucial to create a stable dispersion and allow for the solution-processability of PEDOT:PSS,[8,12] which is the key to its success. There are several formulations of PEDOT:PSS widely used, which may be categorized as two main types based on the applications: (1) for conductive electrodes, such as Clevios P, PH500, and PH1000, with a typical PEDOT:PSS weight ratio of 1:2.5 and conductivity in the range of 0.1 to 1 S cm^{-1}; and (2) for HTL, in particular Clevios P VP AI 4083, with a typical PEDOT:PSS weight ratio of 1:6 and conductivity of 10^{-3} to 10^{-4} S cm^{-1}.[10] More PSS is present in the latter to improve the processability and achieve a high work function. It is evident that the conductivity is lower as a result; however, specifically for the HTL application, conductivity is not necessarily the first priority.

As PEDOT:PSS was first developed as an electrically conducting polymer, many reports focus on increasing its conductivity, particularly for electrode applications to reach 100-1000 S cm^{-1} or higher.[9,10,13] One of the most versatile routes is to utilize additives, such as organic solvents, ionic liquids, zwitterions, surfactants, salts, and acids, by either adding them

to the initial processing solution or conducting a post-deposition treatment.[14–21] Interestingly, the general mechanism to improve the conductivity is based on the removal of the insulating PSS part from the final film. It is generally demonstrated that the conductivity-enhancement procedures lead to some elimination of the excess PSS and results in the phase separation between the PEDOT-rich part and the insulating PSS-rich part. The PEDOT-rich part can then form a conducting network which improves the conductivity drastically.[11,22] At the microscopic level, the conformation of the PEDOT chain can also change to allow for higher carrier mobility as well.[23]

However, when PEDOT:PSS is employed as the HTL, particularly for PV applications, increasing the conductivity does not always lead to higher PV efficiency.[18,24–26] This is because the HTL is relatively thin compared to the overall device, and many factors can affect the efficiency, such as energy level alignment, optical transparency, and film morphology. Recently, it has been shown that 'dedoping' PEDOT:PSS with NaOH can improve the performance of perovskite solar cells (PSCs) even when the conductivity of the PEDOT:PSS layer is in fact lower.[26] In this work, we employ tin(II) thiocyanate [$Sn(SCN)_2$] as an additive to dedope PEDOT:PSS and fine-tune the properties of the HTL for OPVs. While the conductivity is slightly reduced, the transport properties improve which result in a higher power conversion efficiency (PCE).

Metal thiocyanate (MSCN) coordination polymers have recently shown strong potential for electronic and optoelectronic applications, particularly copper(I) thiocyanate (CuSCN).[27–33] Other MSCNs also offer a rich variety of structural, chemical, and electronic properties.[34] Among the MSCNs, $Sn(SCN)_2$ has emerged as one of the promising coordination polymer semiconductors for OPVs owing to its simple solution processibility and solvent orthogonality with the organic layers.[35,36] More specifically, $Sn(SCN)_2$ is processable in common polar solvents, such as alcohols, which is in contrast to CuSCN that requires sulfur or nitrogen-containing solvents.[37,38]

We have recently demonstrated that the ultrathin $Sn(SCN)_2$ films can be employed as anode interlayers in OPV devices that can effectively contain excitons and reduce the recombination loss, resulting in an average PCE of 7.6% (maximum = 8.1%) for optimized cells based on poly[4,8-bis(5-(2-ethylhexyl)thiophen-2-yl)benzo[1,2-b;4,5-b']dithiophene-2,6-diyl-alt-(4-(2-ethylhexyl)-3-fluorothieno[3,4-b]thiophene-)-2-carboxylate-2-6-diyl)] (PTB7-Th) and [6,6]-phenyl-C_{71}-butyric acid methyl ester ($PC_{71}BM$) as the bulk heterojunction (BHJ) layer.[36] Furthermore, $Sn(SCN)_2$ has also been reported as an additive for electron-transporting small molecules in OPVs by Seitkhan et al.[39] The hybrid electron transporting layer (ETL) exhibits significant enhancements in device performance for both OPVs and PSCs. Due to the processability of $Sn(SCN)_2$ in alcohols, it is therefore of great interest to investigate its use as an additive in the quintessential HTL — PEDOT:PSS.

Herein, we show that adding $Sn(SCN)_2$ to PEDOT:PSS HTL can enhance the hole transport properties and the corresponding device performance of OPV cells. PTB7-Th:$PC_{71}BM$ blend is employed as the BHJ layer due to its well-established recipe and known characteristics. At the optimal doping concentration of 0.15% w/v, the average PCE increases from 9.0% to 9.8% due to a substantial increase in the short-circuit current associated with improved charge carrier transport in the $Sn(SCN)_2$-added PEDOT:PSS layer.

2. Results and discussion

The PEDOT:PSS solutions containing 0.05, 0.10, 0.15, and 0.20% w/v $Sn(SCN)_2$ were first prepared by adding solutions of $Sn(SCN)_2$ in 1-propanol at different concentrations to a commercial PEDOT:PSS solution at a fixed volume ratio (Fig. 1a). A reference solution for chemical analysis was prepared by adding neat 1-propanol to the latter. These solutions were used for depositing film samples by either spin-coating or drop-casting. The full experimental section is included in the Electronic Supplementary Information (ESI).

2.1. Chemical states analysis

Raman spectroscopy was performed to study the effects of $Sn(SCN)_2$ addition on the chemical properties of the PEDOT:PSS films. Note that drop-cast samples were employed to increase the signal intensity in this experiment. As shown in Fig. 1b, the main vibrational peaks of the PEDOT part are located at 1435, 1366, 1261, 1095, and 990 cm^{-1}, which can be attributed to the $C_\alpha=C_\beta$ symmetric stretching, $C_\beta–C_\beta$ stretching, $C_\alpha–C_{\alpha'}$ inter-ring stretching, C–O–C deformation, and oxyethylene ring deformation modes, respectively.[40,41] The complex profile in the range 1470-1600 cm^{-1} is related to the $C_\alpha=C_\beta$ asymmetric stretching which is split into multiple peaks when PEDOT is doped via oxidation (with PSS in this case).[42,43] The signals of the PSS part are found at 1130 and 1040 cm^{-1}, associated with the SO_3^- asymmetric and symmetric stretching modes, respectively.[44–46]

When added with $Sn(SCN)_2$, the main PEDOT peak at 1435 cm^{-1} of the pristine sample is slightly shifted to lower wavenumbers (1429 cm^{-1} at 0.20% w/v) and becomes narrower (full width at half maximum FWHM decreasing from 61 to 37 cm^{-1}). The shift can be ascribed to the conformational change of the PEDOT chain in which some parts with the benzoid structure transform into the quinoid structure (Fig. 1c), likely associated with the dedoping effect that would see some of the bipolaron states (benzoid structure) turning into the polaron states (quinoid structure).[40,41] Changes in the Raman bands of the $C_\alpha=C_\beta$ asymmetric stretching also strongly support this point. With the increasing $Sn(SCN)_2$ concentration, the profile appears less complex, and the peak around 1515 cm^{-1} appears, which can be assigned to the dedoped PEDOT.[41,42] Concomitantly, the signals of the PSS part become relatively weaker. Fig. 1d shows the close-up of the data in the spectral regions of the PSS SO_3^- stretching and PEDOT $C_\alpha=C_\beta$ symmetric stretching to highlight the dedoping effects of $Sn(SCN)_2$. It can be inferred that adding $Sn(SCN)_2$ leads to some removal of the PSS component, which is further confirmed below. The changes and interpretation are consistent with the previous in-situ spectroelectrochemical studies and recent reports on PEDOT:PSS dedoping.[26,40,41,47,48] We note that adding the neat solvent

also shows somewhat similar effects,[49] but to a much lesser degree in our case due to the small amount used.

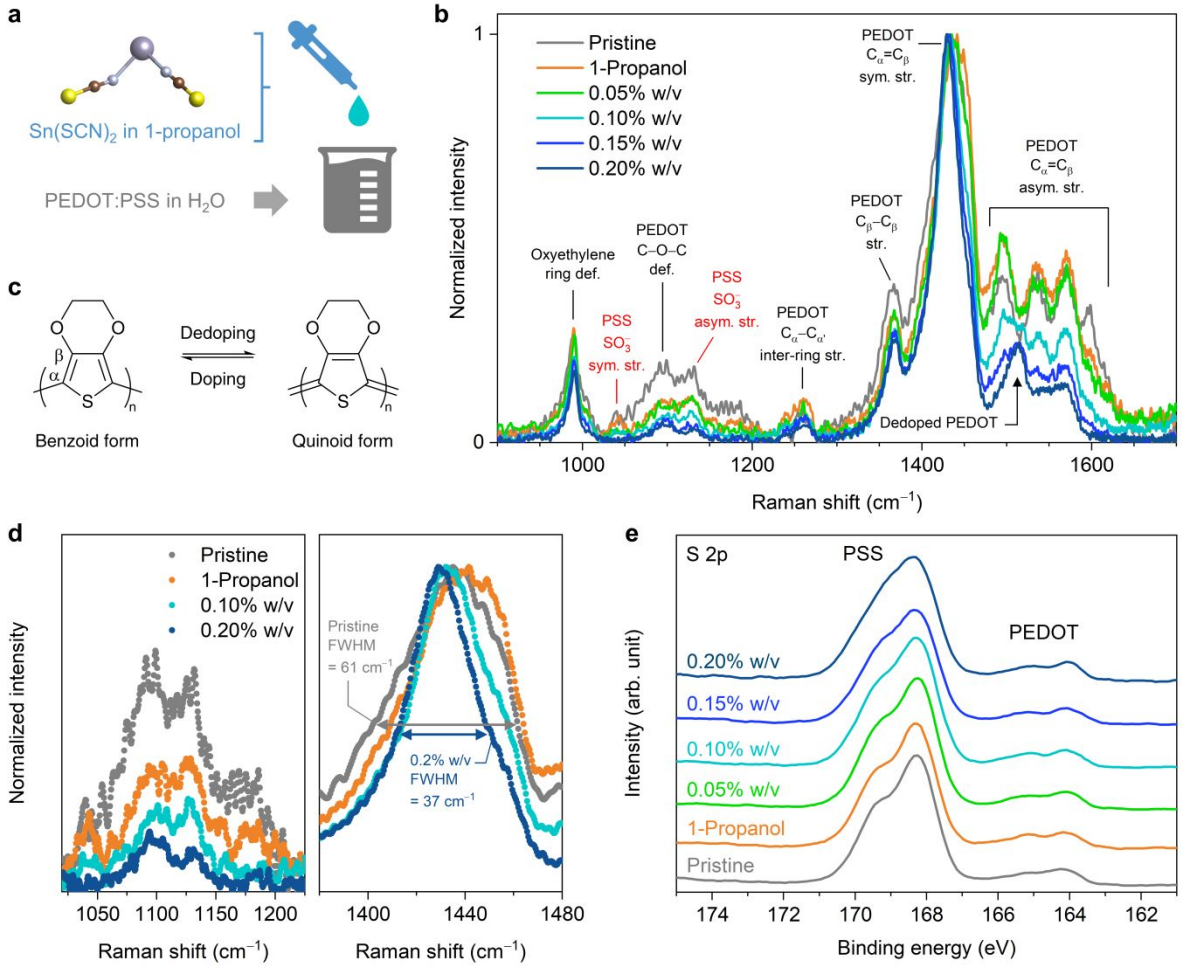

Fig. 1 (a) Process of adding $Sn(SCN)_2$ dissolved in 1-propanol to the solution of PEDOT:PSS in H_2O. (b) Raman spectra (sym. symmetric, asym. asymmetric, str. stretching, and def. deformation) (c) Schematic showing the benzoid and quinoid forms of the main PEDOT chain. (d) Close-up of the Raman spectra. (e) S 2p XPS spectra.

X-ray photoelectron spectroscopy (XPS) was also performed to investigate the chemical composition of PEDOT:PSS samples. The wide scans (Fig. S1, ESI) validate the presence of $Sn(SCN)_2$ as evident from the Sn 3p, 3d, and 4d peaks. This confirms that $Sn(SCN)_2$ is incorporated into the final PEDOT:PSS films after the processing steps. Na is also detected in all samples, likely as a residue from the synthesis of PEDOT:PSS.[50] The narrow scans of the core-level S 2p spectra exhibit two distinct bands as shown in Fig. 1e.

The doublet peaks with binding energies of 163-166 eV are associated with sulfur atoms in PEDOT whereas the band at higher energies of 167-171 eV can be ascribed to sulfur atoms in the PSS.[11] The three oxygen atoms bonded directly to the sulfur of the sulfonate group increase the binding energy significantly, allowing the clear distinction. The compositional modification of the films can be determined by the ratio of the integrated S 2p peak areas of PEDOT to PSS components which is summarized in Table S1 (ESI). The pristine PEDOT:PSS film shows a PEDOT-to-PSS ratio of 0.134, which slightly increases to 0.138 when added with the neat 1-propanol solvent. The incorporation of $Sn(SCN)_2$ results in further removal of PSS as the PEDOT-to-PSS ratio increases to 0.141, 0.147, 0.163, and 0.182 with the increasing additive concentration. The XPS data well corroborates the results of the Raman spectroscopy discussed above.

The removal of PSS upon the treatment with ionic compounds (either by adding directly to the solution or carrying out a post-deposition procedure) is well known in the literature.[16–18,20,25] The mechanism is based on the charge-screening effect of the ionic additive, which leads to the 'decoupling' of the negatively charged PSS (PSS^-) from the positively charged PEDOT ($PEDOT^+$) moieties. Subsequently, whether the added salts can increase or decrease the conductivity depends largely on the specific cations and anions which will be discussed below.

2.2. Optical, electronic, and structural properties

The optical properties of the samples were characterized by ultraviolet-visible-near infrared (UV-Vis-NIR) spectroscopy. Fig. S2 (ESI) presents the optical transmission spectra of pristine and $Sn(SCN)_2$-added PEDOT:PSS films. All films show high transparency of >95% in the visible region (400-700 nm). However, differences in the spectra can be observed in the UV and NIR regions. Below 400 nm, the addition of $Sn(SCN)_2$ noticeably increases the transmittance. Fig. 2a displays the (reflection-corrected) optical absorption in the UV range. The band located at 225 nm can be ascribed to the absorption by the

aromatic rings of the PSS part.[51] The peak intensity decreases with the increasing $Sn(SCN)_2$ concentration, also consistent with the removal of PSS from the PEDOT:PSS films.[20] The absorption spectra in the visible and NIR range are displayed in Fig. 2b. The data are normalized to the minimum absorption around 470 nm to allow a clear comparison of NIR absorption. The increasing amount of $Sn(SCN)_2$ results in a decrease in the absorbance at wavelengths longer than 1000 nm (energy < 1.2 eV) and simultaneously an emergence of a broad peak around 900 nm (energy ≈ 1.4 eV). The former can be assigned to a bipolaron state (lower transition energy) and the latter to a polaron state (slightly higher transition energy).[52] The changes in the optical spectra therefore strongly indicate the dedoping effect (a decrease in the number of positive charges on PEDOT as bipolarons turn into polarons).[26,47] The conformational change from the benzoid form (bipolaron state) to the quinoid form (polaron state) seen in Raman spectroscopy results (Section 2.1) also substantiates this point according to earlier spectroelectrochemical studies.[40,41] Furthermore, the absence of an absorption band around 600 nm, which corresponds to the π- π* transition of the neutral PEDOT,[40,41] suggests that the PEDOT chains in our samples are still moderately doped. In short, when added with $Sn(SCN)_2$, some PSS is decoupled from the PEDOT chains, and the degree of PEDOT doping/oxidation becomes lower/reduced (but does not reach zero).

The electronic properties of the samples were also studied by photoelectron yield spectroscopy (PYS) and Kelvin probe (KP) measurements, which allow the determination of the valence energy level E_V and the work function or Fermi level E_F. The optical band gap E_g^{opt} was calculated from the UV-Vis-NIR absorption spectra, and the conduction energy level E_C can be calculated from $E_V + E_g^{opt}$. The schematic energy diagrams shown in Fig. S3 (ESI) also confirm the dedoping effect as seen from the shift of E_F away from E_V with the increasing concentration of $Sn(SCN)_2$, further corroborating the decrease in the number of positive charge carriers discussed above. Specifically, $|E_F - E_V|$ gradually increases from 0.02 eV for pristine PEDOT:PSS to 0.38 eV for PEDOT:PSS added with 0.20% w/v

$Sn(SCN)_2$. The optical and electronic properties of modified PEDOT:PSS films are well correlated with the chemical properties presented in the previous section.

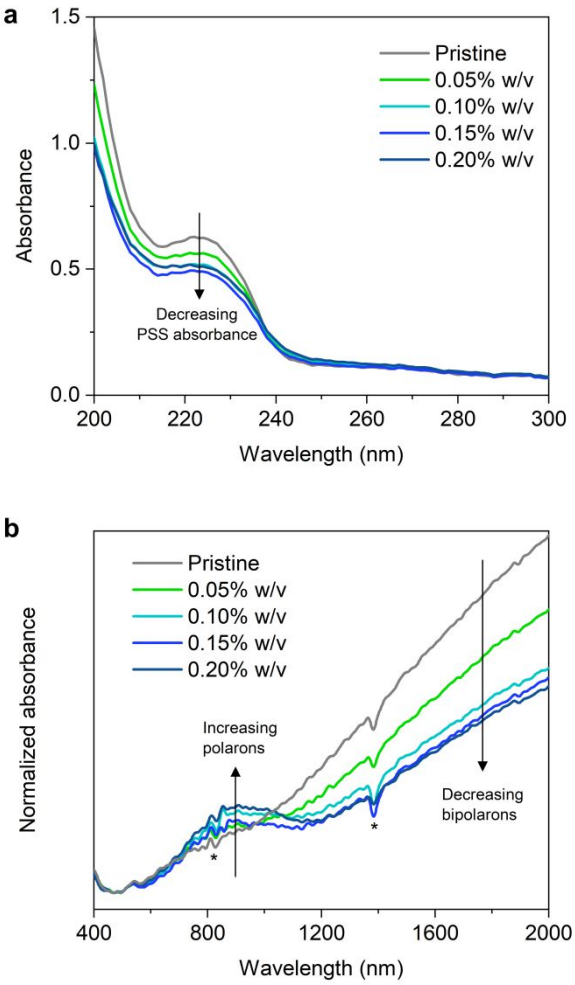

Fig. 2 Optical absorption spectra in the (a) UV and (b) NIR regions. Asterisks (*) denote the instrumental artifacts from the measurements.

To investigate the effects of $Sn(SCN)_2$ addition on the structural properties of PEDOT:PSS films, the samples were prepared by drop-casting and analyzed by X-ray diffraction (XRD) as presented in Fig. 3a. The two characteristic peaks at 17.7° and 25.0° can be assigned to the π-π stackings of the PSS and PEDOT components, respectively.[53,54] With the increasing $Sn(SCN)_2$ concentration, the peak intensity at 2θ = 17.7° significantly decreases owing to the loss of PSS. Furthermore, the $Sn(SCN)_2$-added PEDOT:PSS films exhibit slightly higher intensity at the low angle diffraction particularly around 2θ = 4° as

shown in Fig. 3b. The diffraction in this region is related to the lamella stacking distance in the (100) direction [$d_{(100)}$] of the alternate ordering between the PEDOT and PSS chains [$d_{(100)}$ ≈ 22-23 Å].[55,56] The higher intensity indicates an increase in the ordering upon the addition of $Sn(SCN)_2$. A close analysis of the PEDOT π-π stacking distance in the (010) direction [$d_{(010)}$] is also shown in Fig. 3c. It can be observed that the diffraction peak is shifted slightly from 24.96° to 25.36°, corresponding to $d_{(010)}$ decreasing from 3.56 to 3.51 Å. The higher order and shorter PEDOT π-π distance facilitate interchain transport and generally leads to higher carrier mobility,[55,56] which we confirm in the next section. The changes in the film structural properties can be ascribed to the more planar molecular structure of the quinoid form which results from the addition of $Sn(SCN)_2$, consistent with the Raman spectroscopy data. Similar observations have been reported for other additives.[15,57,58]

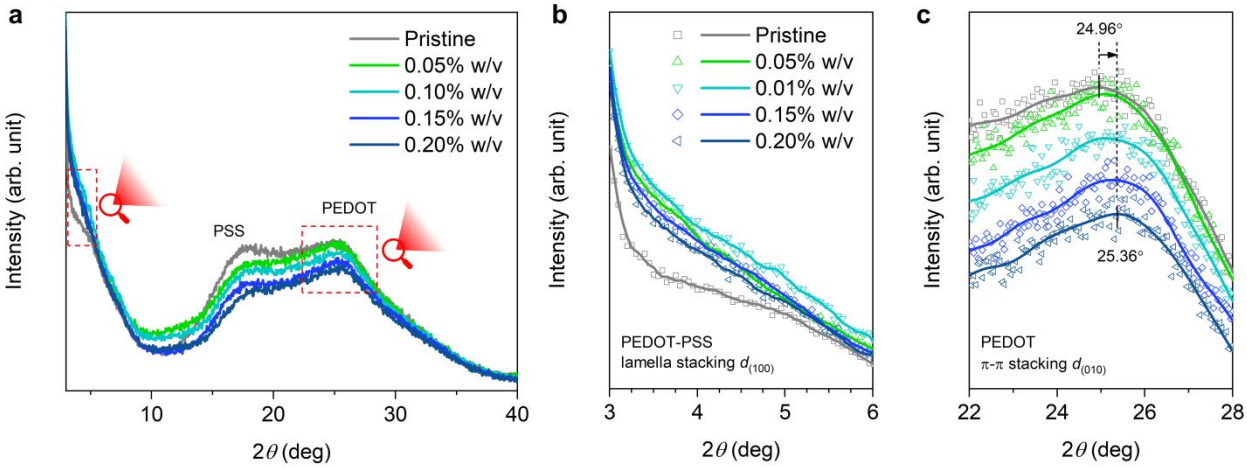

Fig. 3 (a) XRD patterns with the close-up of the regions marked with red dashed boxes shown in (b) and (c).

2.3. Carrier mobility, electrical conductivity, and discussion on dedoping effects

The charge carrier transport properties of $Sn(SCN)_2$-added PEDOT:PSS films were measured using time-resolved microwave conductivity (TRMC). All samples were prepared on quartz substrates and excited with a Nd:YAG laser source (second harmonic, 532 nm). The transient photoconductivity ($\Delta\sigma_{TRMC}$) is correlated to a product of charge carrier generation

quantum efficiency (ϕ) and the sum of charge carrier mobilities ($\Sigma\mu$) or $\phi\Sigma\mu$ (more information in the ESI). The time-resolved data of $\phi\Sigma\mu$ are plotted in Fig. S4 (ESI), showing that the photoconductivity consistently increases with higher $Sn(SCN)_2$ concentrations. The peak values $\phi\Sigma\mu_{max}$ are summarized in Fig. 4a. As the optical properties of the films are similar at the excitation wavelength, the increase in the TRMC signal indicates an enhancement of hole mobility in the PEDOT:PSS layer. As described in the previous section, this is fully consistent with the structural changes in the film that give rise to higher crystallinity and closer PEDOT π-π distance which improves interchain carrier transport.[47,54–56]

The electrical conductivity (σ) of the PEDOT:PSS samples were measured with a four-point probe method, and the results are plotted in Fig. 4b. The pristine PEDOT:PSS shows a σ value of 1.7×10^{-3} S cm^{-1}, which is typical of the Clevios P VP AI 4083 grade used in this work.[10,13] Initially, σ increases to 2.5×10^{-3} S cm^{-1} at 0.05% w/v of $Sn(SCN)_2$ but then decreases with higher $Sn(SCN)_2$ concentration. At 0.20% w/v, σ is measured to be 1.1×10^{-3} S cm^{-1}, slightly lower than the pristine sample. This trend in the electrical conductivity may appear perplexing at first; however, when considering that $\sigma = qn\mu$, where q is the elementary charge, n is the carrier concentration, and μ is the charge carrier mobility, the observed trend in σ can be explained. Despite the monotonic increase in μ as characterized by TRMC, which should lead to a concurrent increase in σ, the other parameter n in fact decreases due to the dedoping effect as evident from the UV-Vis-NIR results (Section 2.2). The absorption in the NIR range which corresponds to conducting charges significantly decreases with the increasing amount of $Sn(SCN)_2$, indicating a reduction in the carrier concentrations. Essentially, there is a trade-off between μ and n. At 0.05% w/v, the increase in μ dominates and leads to the slight increase in σ. At higher concentrations, the decrease in n becomes dominant which is reflected in the smaller σ.

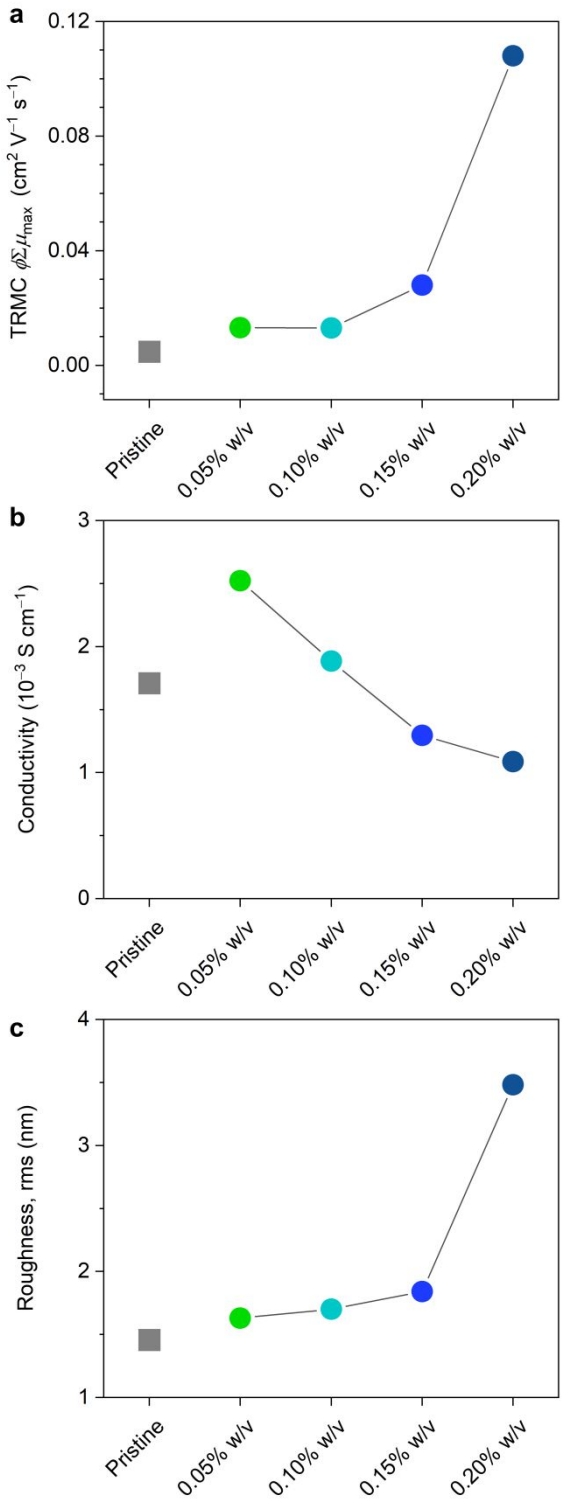

Fig. 4 (a) Figure of merit from time-resolved microwave conductivity (TRMC), (b) film conductivity, and (c) root-mean-square (rms) roughness of pristine and $Sn(SCN)_2$-added PEDOT:PSS films.

We characterized the samples further by examining the film morphology using atomic force microscopy (AFM). The samples were spin-coated onto ITO substrates (having the

same anode/HTL stack as in the OPV devices as presented in the next section). At the 5×5 μm^2 image size (Fig. S5, ESI), the nanoscale morphology is similar for all samples. When observing the larger 20×20 μm^2 image size (Fig. S6, ESI), some variation in the film uniformity can be observed. Specifically, more aggregation is seen with the increasing $Sn(SCN)_2$ concentration, likely related to the tendency of $Sn(SCN)_2$ to coalesce and form particles due to the high coordination number of Sn and abundant Sn···S interactions in the structure as described in our previous studies.[35,36] The root-mean-square roughness (σ_{rms}) obtained from the large image size, which better represents the device-relevant morphology, shows an increasing trend with the larger amount of $Sn(SCN)_2$ as plotted in Fig. 4c. For the pristine sample and $Sn(SCN)_2$ concentration up to 0.15% w/v (which is the optimal condition for OPV as shown next), the AFM analysis confirms the favorable smoothness with σ_{rms} < 2 nm. At 0.20% w/v, σ_{rms} increases to 3.5 nm (slightly higher than glass and ITO which have σ_{rms} of around 2 and 3 nm, respectively), and large particles appear. The film thicknesses of the PEDOT:PSS samples were also measured by profilometry. The pristine film has a thickness of 54 nm, and upon the addition of $Sn(SCN)_2$ at 0.05% w/v, the thickness drops to 43 nm, likely due to the loss of some PSS as mentioned above. Higher amount of $Sn(SCN)_2$ gradually increases the thickness to 44, 47, and 48 nm for 0.10, 0.15, and 0.20% w/v, respectively, which we ascribe to the increasing amount of $Sn(SCN)_2$.

We can summarize the effects of adding $Sn(SCN)_2$ as follows. XPS confirms that $Sn(SCN)_2$ is incorporated into the final PEDOT:PSS films and shows that the amount of PSS decreases with the higher $Sn(SCN)_2$ concentrations. Raman spectroscopy substantiates the loss of PSS and, importantly, reveals the dedoping effect: the PEDOT chains become reduced upon the addition of $Sn(SCN)_2$. This is observed as some of the benzoid structure (bipolaron state) transforms into the quinoid structure (polaron state). UV-Vis-NIR spectroscopy further confirms the partial PSS removal (lower UV absorption) and the decrease in the carrier concentrations (lower bipolaron absorption and higher polaron absorption). PYS and KP measurements also corroborate the dedoping effects. XRD then

shows that following the loss of PSS, the PEDOT chains are packed closer together, allowing better carrier transport. As a result, TRMC shows the increasing hole mobility when $Sn(SCN)_2$ is added. The trend in the conductivity can be explained based on the trade-off between the increasing mobility and the decreasing carrier concentration.

Previous reports show that adding or treating PEDOT:PSS with some salts can lead to a large increase in the conductivity (so-called 'secondary doping' effect).[9,17,20,57,59] However, such an increase is accompanied by dramatic changes in other physical properties of the PEDOT:PSS films. Specifically, the loss of PSS is much more significant, and the procedure typically leads to a distinct phase separation between the conductive PEDOT regions and the insulating PSS regions.[60,61] In such cases, the PEDOT can form an efficient conducting network. However, in our case, the macroscopic phase separation does not occur as evident from the AFM results. Also, whether or not the salts lead to the secondary doping effect depends on the specific cations and anions. Ouyang et al. reported that cations with a high positive softness parameter are required to bind with PSS^- (to effectively remove PSS from PEDOT) and that anions with a high dissociation constant (low pKa of the conjugate acid) are necessary for binding with $PEDOT^+$ to retain the high doping level, for example, $CuCl_2$, $CuBr_2$, $InCl_3$, $InBr_3$, and InI_3.[17,20] For $Sn(SCN)_2$, Sn^{2+} is a soft cation, but SCN^- has a lower tendency to dissociate compared to Cl^-, Br^-, or I^- as the pKa of HSCN (pKa = 0.85) is much higher than those of HCl, HBr, or HI (pKa = -8, -9, and -10, respectively).[62,63] Therefore, it is consistent that SCN^- cannot effectively dope PEDOT, resulting in the observed dedoping effects shown in this work.

2.4. Application in organic photovoltaics

To demonstrate the OPV applications, solar cells were fabricated using PTB7-Th:PC71BM as a donor:acceptor pair in the BHJ layer, indium tin oxide (ITO) as an anode, bathocuproine (BCP) as a cathode interlayer, and Al as a cathode. For different samples, pristine or $Sn(SCN)_2$-added PEDOT:PSS was utilized as the HTL. We note also that the pH

of the HTL solutions became higher (less acidic) when $Sn(SCN)_2$ was added (Table S1, ESI). Fig. 5a shows the schematic OPV structure; the cells had an active area of 0.0707 cm^2. The relevant schematic energy diagram is illustrated in Fig. 5b using values from our measurements for PEDOT and from the literature for other layers.[36,64] The representative current density-voltage (*J-V*) characteristics (AM1.5G, 1 sun intensity) of the OPV devices in which the PEDOT:PSS HTL was modified with different $Sn(SCN)_2$ concentrations are presented in Fig. 5c. All device parameters and statistics from 10 OPV cells for each condition are listed in Table S2 (ESI) and shown as box plots in Fig. S7 (ESI).

The OPV devices with the pristine PEDOT:PSS as the HTL show a PCE of 8.99%, a short circuit current (J_{sc}) of 15.94 mA cm^{-2}, an open circuit voltage (V_{oc}) of 0.809 V, and fill factor (FF) of 69.8% (all average values). Modifying PEDOT:PSS with a small amount of $Sn(SCN)_2$ can significantly improve the OPV performance. The optimal concentration is 0.15% w/v of $Sn(SCN)_2$ yielding an average PCE of 9.77% (J_{sc} = 17.06 mA cm^{-2}, V_{oc} = 0.809 V, and FF = 72.9%), and a maximum PCE of 9.90%. We also note that the 0.20%w/v condition leads to slightly lower performance, likely due to the higher roughness of the HTL (Fig. 4c) which can impede hole extraction across the interface. It can be observed that FF increases in all cases, and the enhancement in PCE is reflected in the trend of J_{sc}.

To investigate the J_{sc} improvement, the external quantum efficiency (EQE) of the solar cells were measured, and the results are plotted in Fig. 5d. All conditions exhibit similar spectral features, but the optimal $Sn(SCN)_2$ condition (0.15% w/v) significantly improves the EQE by 3-4% across 350-750 nm compared to the cell based on pristine PEDOT:PSS. The integration of the measured EQE yields photocurrent values of 15.5 (pristine), 15.9 (0.05% w/v), 16.2 (0.10% w/v), 16.3 (0.15% w/v), and 15.7 mA cm^{-2} (0.20% w/v), which are in good agreement with the J_{sc} values obtained from the *J-V* characteristics (see Table S2). Since the BHJ active layer is identical, the reason for the increased J_{sc} lies in the improved carrier transport through the HTL.

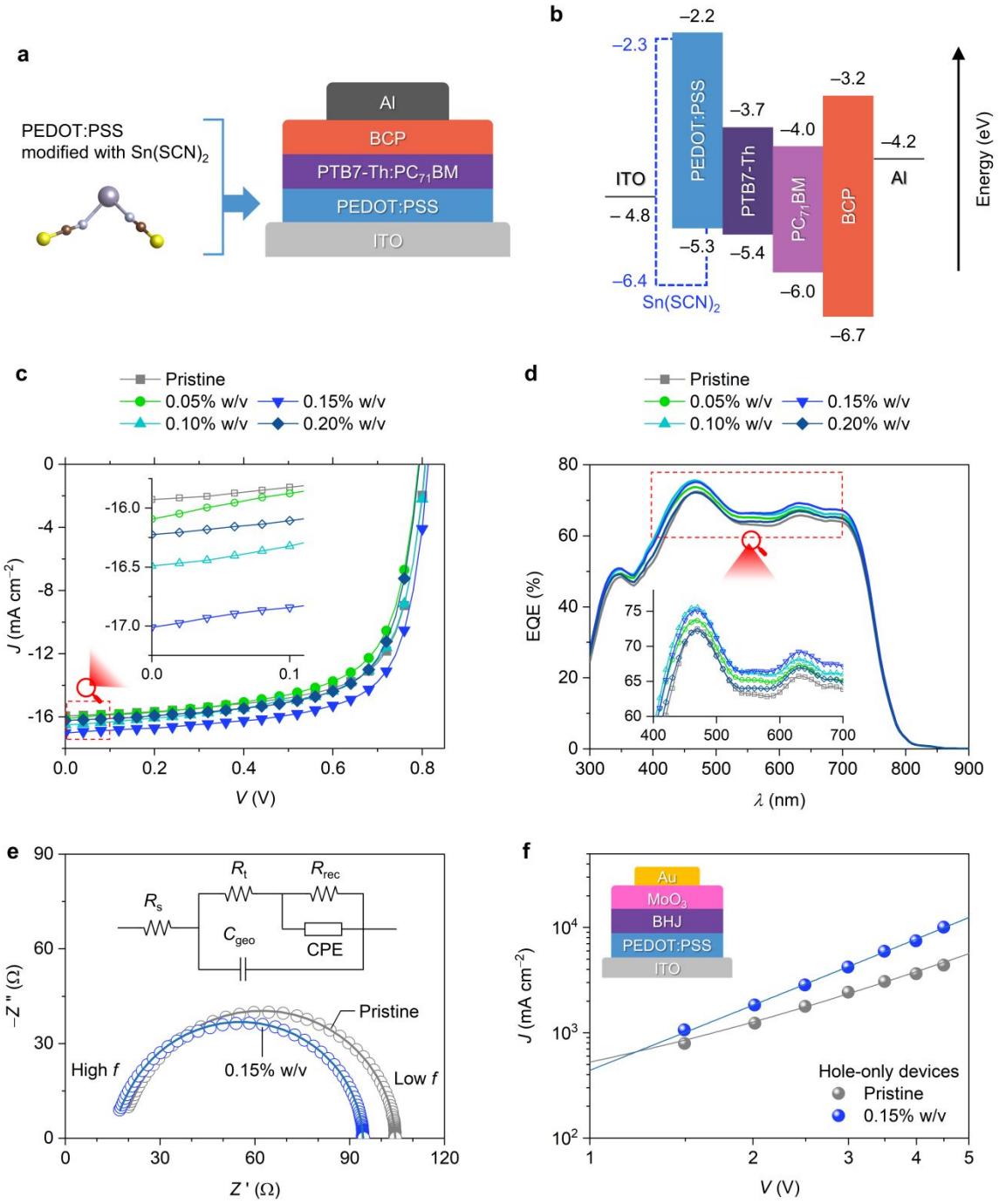

Fig. 5 (a) Schematic diagram of OPV structure. (b) Schematic energy diagrams of the OPV layers. (c) Current density-voltage (*J*-*V*) characteristics of representative OPV cells. (d) External quantum efficiency (EQE) spectra. The insets in (c) and (d) show magnified views of the regions marked by the red dashed boxes. (e) Nyquist plots of impedance spectroscopy with the inset showing the equivalent circuit for a BHJ device. (f) *J*-*V* characteristics of the hole-only devices with the inset showing the device structure.

To elucidate the differences, the solar cell devices based on the pristine and 0.15% w/v $Sn(SCN)_2$-added PEDOT:PSS HTLs (control *vs* optimal conditions) were further characterized using electrochemical impedance spectroscopy (EIS). Based on the impedance model of BHJ devices,[65,66] since the BHJ layer in this work is fixed for all samples, the recombination kinetics is expected to be similar; the parameters of interest herein are therefore the contact resistance (R_c) and particularly the transport resistance (R_t), the latter of which refers to the resistance of charge extraction across the devices. We obtained these values by carrying out the EIS under dark condition with a forward dc bias of 0.8 V (near V_{oc}) and fitting the data with the abovementioned model. Fig. 5e shows the Nyquist plots (symbols) and fitting data (solid lines) calculated from the equivalent circuit as illustrated in the inset. The fitting results are reported in Table S3 (ESI). Apparently, R_c and R_t both decrease from 16.9 and 67.5 Ω (pristine PEDOT:PSS) to 14.5 and 62.4 Ω [0.15% w/v $Sn(SCN)_2$], suggesting that an optimal concentration of $Sn(SCN)_2$ can promote the charge extraction from the device.

The electrical properties of the HTLs were additionally investigated by determining the overall hole mobility using the space charge limited current (SCLC) analysis. Hole-only devices comprising ITO/HTL/BHJ/MoO_3/Au were fabricated for this measurement, and two HTLs similar to the EIS experiment were compared as shown in Fig. 5f. The values of SCLC hole mobilities ($\mu_{h,SCLC}$) were determined using the Murgatroyd equation[67,68] as summarized in Table S4 (ESI). Notably, $\mu_{h,SCLC}$ increases from 3.67×10^{-5} cm^2 V^{-1} s^{-1} (pristine PEDOT:PSS HTL) to 4.17×10^{-5} cm^2 V^{-1} s^{-1} [0.15% w/v $Sn(SCN)_2$-added HTL]. The result further corroborates that adding $Sn(SCN)_2$ to PEDOT:PSS can improve the charge carrier transport that ultimately leads to higher efficiency. The solutions of $Sn(SCN)_2$-added PEDOT:PSS are also stable as no phase separation or precipitation can be observed as shown in Figure S8 (ESI).

3. Conclusions

We demonstrate that $Sn(SCN)_2$ can be used as an additive to improve the hole transport properties of the standard PEDOT:PSS films. The incorporation of $Sn(SCN)_2$ leads to slight dedoping from the separation of the PSS part from the PEDOT chain due to the screening effect. The improved PEDOT packing leads to a higher hole mobility. At the optimal $Sn(SCN)_2$ concentration of 0.15% w/v, the OPV cells show higher J_{sc} that contributes to an increase in the average PCE from 9.0% to 9.8%. A higher additive amount then causes aggregation and higher film roughness that reduces the OPV efficiency. This work demonstrates that fine-tuning the properties of the PEDOT:PSS HTL by dedoping can further improve the OPV performance.

Author contributions

Jidapa Chaopaknam: methodology, investigation, formal analysis, validation, visualization, and writing – original draft. **Taweesak Sudyoadsuk**: methodology and supervision. **Vinich Promarak**: resources and funding acquisition. **Akinori Saeki**: methodology, validation, supervision, resources, and writing – review & editing. **Pichaya Pattanasattayavong**: conceptualization, funding acquisition, resources, supervision, validation, visualization, writing – review & editing, and project administration.

Conflicts of interest

There are no conflicts to declare.

Acknowledgements

This research is funded by National Research Council of Thailand (NRCT), grant no. N42A650255 and N42A650196, and Thailand Science Research and Innovation (TSRI), grant no. FRB660004/0457. This material is based upon work supported by the Air Force Office of Scientific Research under award number FA2386-22-1-4082. J.C. and P.P. acknowledge Vidyasirimedhi Institute of Science and Technology (VISTEC) for PhD scholarship and research funding and VISTEC's Frontier Research Center (FRC) for scientific instruments. A.S. acknowledges the support from Japan Society for the Promotion of Science (JSPS) (grant no. JP20H05836). Dr. Somlak Ittisanronnachai and Dr. Pimpisut Worakajit from VISTEC are acknowledged for their help with additional XPS measurements and analyses. Asst. Prof. Dr. Kanokwan Kongpatpanich, VISTEC, is thanked for allowing the use of the pH meter.

References

(1) Zhang, M.; Zhu, L.; Zhou, G.; Hao, T.; Qiu, C.; Zhao, Z.; Hu, Q.; Larson, B. W.; Zhu, H.; Ma, Z.; Tang, Z.; Feng, W.; Zhang, Y.; Russell, T. P.; Liu, F. Single-Layered Organic Photovoltaics with Double Cascading Charge Transport Pathways: 18% Efficiencies. *Nat. Commun.* **2021**, *12*, 309.

(2) Bi, P.; Zhang, S.; Chen, Z.; Xu, Y.; Cui, Y.; Zhang, T.; Ren, J.; Qin, J.; Hong, L.; Hao, X.; Hou, J. Reduced Non-Radiative Charge Recombination Enables Organic Photovoltaic Cell Approaching 19% Efficiency. *Joule* **2021**, *5*, 2408–2419.

(3) Zhan, L.; Li, S.; Li, Y.; Sun, R.; Min, J.; Bi, Z.; Ma, W.; Chen, Z.; Zhou, G.; Zhu, H.; Shi, M.; Zuo, L.; Chen, H. Desired Open-Circuit Voltage Increase Enables Efficiencies Approaching 19% in Symmetric-Asymmetric Molecule Ternary Organic Photovoltaics. *Joule* **2022**, *6*, 662–675.

(4) Firdaus, Y.; Le Corre, V. M.; Khan, J. I.; Kan, Z.; Laquai, F.; Beaujuge, P. M.;

Anthopoulos, T. D. Key Parameters Requirements for Non-Fullerene-Based Organic Solar Cells with Power Conversion Efficiency >20%. *Adv. Sci.* **2019**, *6*, 1802028.

(5) Karki, A.; Gillett, A. J.; Friend, R. H.; Nguyen, T. The Path to 20% Power Conversion Efficiencies in Nonfullerene Acceptor Organic Solar Cells. *Adv. Energy Mater.* **2021**, *11*, 2003441.

(6) Yip, H.-L.; Jen, A. K. Y. Recent Advances in Solution-Processed Interfacial Materials for Efficient and Stable Polymer Solar Cells. *Energy Environ. Sci.* **2012**, *5*, 5994.

(7) Yin, Z.; Wei, J.; Zheng, Q. Interfacial Materials for Organic Solar Cells: Recent Advances and Perspectives. *Adv. Sci.* **2016**, *3*, 1500362.

(8) Jonas, F.; Krafft, W.; Muys, B. Poly(3, 4-Ethylenedioxythiophene): Conductive Coatings, Technical Applications and Properties. *Macromol. Symp.* **1995**, *100*, 169–173.

(9) Ouyang, J. “Secondary Doping” Methods to Significantly Enhance the Conductivity of PEDOT:PSS for Its Application as Transparent Electrode of Optoelectronic Devices. *Displays* **2013**, *34*, 423–436.

(10) Shi, H.; Liu, C.; Jiang, Q.; Xu, J. Effective Approaches to Improve the Electrical Conductivity of PEDOT:PSS: A Review. *Adv. Electron. Mater.* **2015**, *1*, 1500017.

(11) Crispin, X.; Marciniak, S.; Osikowicz, W.; Zotti, G.; van der Gon, A. W. D.; Louwet, F.; Fahlman, M.; Groenendaal, L.; De Schryver, F.; Salaneck, W. R. Conductivity, Morphology, Interfacial Chemistry, and Stability of Poly(3,4-Ethylene Dioxythiophene)-Poly(Styrene Sulfonate): A Photoelectron Spectroscopy Study. *J. Polym. Sci. Part B Polym. Phys.* **2003**, *41*, 2561–2583.

(12) Groenendaal, L.; Jonas, F.; Freitag, D.; Pielartzik, H.; Reynolds, J. R. Poly(3,4-Ethylenedioxythiophene) and Its Derivatives: Past, Present, and Future. *Adv. Mater.*

2000, *12*, 481–494.

(13) Shahrim, N. A.; Ahmad, Z.; Wong Azman, A.; Fachmi Buys, Y.; Sarifuddin, N. Mechanisms for Doped PEDOT:PSS Electrical Conductivity Improvement. *Mater. Adv.* **2021**, *2*, 7118–7138.

(14) Kim, J. Y.; Jung, J. H.; Lee, D. E.; Joo, J. Enhancement of Electrical Conductivity of Poly(3,4-Ethylenedioxythiophene)/Poly(4-Styrenesulfonate) by a Change of Solvents. *Synth. Met.* **2002**, *126*, 311–316.

(15) Ouyang, J.; Xu, Q.; Chu, C.-W.; Yang, Y.; Li, G.; Shinar, J. On the Mechanism of Conductivity Enhancement in Poly(3,4-Ethylenedioxythiophene):Poly(Styrene Sulfonate) Film through Solvent Treatment. *Polymer* **2004**, *45*, 8443–8450.

(16) Fan, B.; Mei, X.; Ouyang, J. Significant Conductivity Enhancement of Conductive Poly(3,4-Ethylenedioxythiophene):Poly(Styrenesulfonate) Films by Adding Anionic Surfactants into Polymer Solution. *Macromolecules* **2008**, *41*, 5971–5973.

(17) Xia, Y.; Ouyang, J. Salt-Induced Charge Screening and Significant Conductivity Enhancement of Conducting Poly(3,4-Ethylenedioxythiophene):Poly(Styrenesulfonate). *Macromolecules* **2009**, *42*, 4141–4147.

(18) Xia, Y.; Zhang, H.; Ouyang, J. Highly Conductive PEDOT:PSS Films Prepared through a Treatment with Zwitterions and Their Application in Polymer Photovoltaic Cells. *J. Mater. Chem.* **2010**, *20*, 9740.

(19) Xia, Y.; Ouyang, J. Significant Conductivity Enhancement of Conductive Poly(3,4-Ethylenedioxythiophene): Poly(Styrenesulfonate) Films through a Treatment with Organic Carboxylic Acids and Inorganic Acids. *ACS Appl. Mater. Interfaces* **2010**, *2*, 474–483.

(20) Xia, Y.; Ouyang, J. Anion Effect on Salt-Induced Conductivity Enhancement of Poly(3,4-Ethylenedioxythiophene):Poly(Styrenesulfonate) Films. *Org. Electron.* **2010**, *11*, 1129–1135.

(21) Badre, C.; Marquant, L.; Alsayed, A. M.; Hough, L. A. Highly Conductive Poly(3,4-Ethylenedioxythiophene):Poly (Styrenesulfonate) Films Using 1-Ethyl-3-Methylimidazolium Tetracyanoborate Ionic Liquid. *Adv. Funct. Mater.* **2012**, *22*, 2723–2727.

(22) Crispin, X.; Jakobsson, F. L. E.; Crispin, A.; Grim, P. C. M.; Andersson, P.; Volodin, A.; van Haesendonck, C.; Van der Auweraer, M.; Salaneck, W. R.; Berggren, M. The Origin of the High Conductivity of Poly(3,4-Ethylenedioxythiophene)-Poly(Styrenesulfonate) (PEDOT-PSS) Plastic Electrodes. *Chem. Mater.* **2006**, *18*, 4354–4360.

(23) Ouyang, J.; Chu, C.-W.; Chen, F.-C.; Xu, Q.; Yang, Y. High-Conductivity Poly(3,4-Ethylenedioxythiophene):Poly(Styrene Sulfonate) Film and Its Application in Polymer Optoelectronic Devices. *Adv. Funct. Mater.* **2005**, *15*, 203–208.

(24) Xiao, T.; Cui, W.; Anderegg, J.; Shinar, J.; Shinar, R. Simple Routes for Improving Polythiophene:Fullerene-Based Organic Solar Cells. *Org. Electron.* **2011**, *12*, 257–262.

(25) Xia, Y.; Sun, K.; Chang, J.; Ouyang, J. Effects of Organic Inorganic Hybrid Perovskite Materials on the Electronic Properties and Morphology of Poly(3,4-Ethylenedioxythiophene):Poly(Styrenesulfonate) and the Photovoltaic Performance of Planar Perovskite Solar Cells. *J. Mater. Chem. A* **2015**, *3*, 15897–15904.

(26) Chin, Y.-C.; Daboczi, M.; Henderson, C.; Luke, J.; Kim, J.-S. Suppressing PEDOT:PSS Doping-Induced Interfacial Recombination Loss in Perovskite Solar Cells. *ACS Energy Lett.* **2022**, *7*, 560–568.

(27) Qin, P.; Tanaka, S.; Ito, S.; Tetreault, N.; Manabe, K.; Nishino, H.; Nazeeruddin, M. K.; Grätzel, M. Inorganic Hole Conductor-Based Lead Halide Perovskite Solar Cells with 12.4% Conversion Efficiency. *Nat. Commun.* **2014**, *5*, 3834.

(28) Li, M.; Gao, K.; Wan, X.; Zhang, Q.; Kan, B.; Xia, R.; Liu, F.; Yang, X.; Feng, H.; Ni, W.; Wang, Y.; Peng, J.; Zhang, H.; Liang, Z.; Yip, H.-L.; Peng, X.; Cao, Y.; Chen, Y. Solution-Processed Organic Tandem Solar Cells with Power Conversion Efficiencies >12%. *Nat. Photonics* **2017**, *11*, 85–90.

(29) Ding, T.; Wang, N.; Wang, C.; Wu, X.; Liu, W.; Zhang, Q.; Fan, W.; Sun, X. W. Solution-Processed Inorganic Copper(I) Thiocyanate as a Hole Injection Layer for High-Performance Quantum Dot-Based Light-Emitting Diodes. *RSC Adv.* **2017**, *7*, 26322–26327.

(30) Arora, N.; Dar, M. I.; Hinderhofer, A.; Pellet, N.; Schreiber, F.; Zakeeruddin, S. M.; Grätzel, M. Perovskite Solar Cells with CuSCN Hole Extraction Layers Yield Stabilized Efficiencies Greater than 20%. *Science* **2017**, *358*, 768–771.

(31) Pattanasattayavong, P.; Promarak, V.; Anthopoulos, T. D. Electronic Properties of Copper(I) Thiocyanate (CuSCN). *Adv. Electron. Mater.* **2017**, *3*, 1600378.

(32) Chavhan, S. D.; Ou, T. H.; Jiang, M. R.; Wang, C. W.; Jou, J. H. Enabling High-Efficiency Organic Light-Emitting Diode with Trifunctional Solution-Processable Copper(I) Thiocyanate. *J. Phys. Chem. C* **2018**, *122*, 18836–18840.

(33) Worakajit, P.; Sudyoadsuk, T.; Promarak, V.; Saeki, A.; Pattanasattayavong, P. Antisolvent Treatment of Copper(I) Thiocyanate (CuSCN) Hole Transport Layer for Efficiency Improvements in Organic Solar Cells and Light-Emitting Diodes. *J. Mater. Chem. C* **2021**, *9*, 10435–10442.

(34) Wechwithayakhlung, C.; Packwood, D. M.; Harding, D. J.; Pattanasattayavong, P.

Structures, Bonding, and Electronic Properties of Metal Thiocyanates. *J. Phys. Chem. Solids* **2021**, *154*, 110085.

(35) Wechwithayakhlung, C.; Packwood, D. M.; Chaopaknam, J.; Worakajit, P.; Ittisanronnachai, S.; Chanlek, N.; Promarak, V.; Kongpatpanich, K.; Harding, D. J.; Pattanasattayavong, P. Tin(II) Thiocyanate $Sn(NCS)_2$ – a Wide Band Gap Coordination Polymer Semiconductor with a 2D Structure. *J. Mater. Chem. C* **2019**, *7*, 3452–3462.

(36) Chaopaknam, J.; Wechwithayakhlung, C.; Nakajima, H.; Lertvanithphol, T.; Horprathum, M.; Sudyoadsuk, T.; Promarak, V.; Saeki, A.; Pattanasattayavong, P. Tin(II) Thiocyanate Sn(SCN)2 as an Ultrathin Anode Interlayer in Organic Photovoltaics. *Appl. Phys. Lett.* **2021**, *119*, 063301.

(37) Worakajit, P.; Hamada, F.; Sahu, D.; Kidkhunthod, P.; Sudyoadsuk, T.; Promarak, V.; Harding, D. J.; Packwood, D. M.; Saeki, A.; Pattanasattayavong, P. Elucidating the Coordination of Diethyl Sulfide Molecules in Copper(I) Thiocyanate (CuSCN) Thin Films and Improving Hole Transport by Antisolvent Treatment. *Adv. Funct. Mater.* **2020**, *30*, 2002355.

(38) Wang, B.; Nam, S.; Limbu, S.; Kim, J.; Riede, M.; Bradley, D. D. C. Properties and Applications of Copper(I) Thiocyanate Hole-Transport Interlayers Processed from Different Solvents. *Adv. Electron. Mater.* **2022**, *8*, 2101253.

(39) Seitkhan, A.; Neophytou, M.; Kirkus, M.; Abou-Hamad, E.; Hedhili, M. N.; Yengel, E.; Firdaus, Y.; Faber, H.; Lin, Y.; Tsetseris, L.; McCulloch, I.; Anthopoulos, T. D. Use of the Phen-NaDPO:Sn(SCN)2 Blend as Electron Transport Layer Results to Consistent Efficiency Improvements in Organic and Hybrid Perovskite Solar Cells. *Adv. Funct. Mater.* **2019**, *29*, 1905810.

(40) Garreau, S.; Louarn, G.; Buisson, J. P.; Froyer, G.; Lefrant, S. In Situ

Spectroelectrochemical Raman Studies of Poly(3,4-Ethylenedioxythiophene) (PEDT). *Macromolecules* **1999**, *32*, 6807–6812.

(41) Garreau, S.; Duvail, J. L.; Louarn, G. Spectroelectrochemical Studies of Poly(3,4-Ethylenedioxythiophene) in Aqueous Medium. *Synth. Met.* **2001**, *125*, 325–329.

(42) Chiu, W. W.; Travaš-Sejdić, J.; Cooney, R. P.; Bowmaker, G. A. Studies of Dopant Effects in Poly(3,4-Ethylenedi-Oxythiophene) Using Raman Spectroscopy. *J. Raman Spectrosc.* **2006**, *37*, 1354–1361.

(43) Farah, A. A.; Rutledge, S. A.; Schaarschmidt, A.; Lai, R.; Freedman, J. P.; Helmy, A. S. Conductivity Enhancement of Poly(3,4-Ethylenedioxythiophene)-Poly(Styrenesulfonate) Films Post-Spincasting. *J. Appl. Phys.* **2012**, *112*, 113709.

(44) Edwards, H. G. M.; Brown, D. R.; Dale, J. A.; Plant, S. Raman Spectroscopy of Sulfonated Polystyrene Resins. *Vib. Spectrosc.* **2000**, *24*, 213–224.

(45) Alía, J. M.; Edwards, H. G. .; Kiernan, B. M. Raman Spectroscopy of Benzenesulfonic and 4-Toluenesulfonic Acids Dissolved in Dimethylsulfoxide. *Spectrochim. Acta Part A Mol. Biomol. Spectrosc.* **2004**, *60*, 1533–1542.

(46) Parker, S. F.; Zhong, L. Vibrational Spectroscopy of Metal Methanesulfonates: M = Na, Cs, Cu, Ag, Cd. *R. Soc. Open Sci.* **2018**, *5*, 171574.

(47) Park, H.; Lee, S. H.; Kim, F. S.; Choi, H. H.; Cheong, I. W.; Kim, J. H. Enhanced Thermoelectric Properties of PEDOT:PSS Nanofilms by a Chemical Dedoping Process. *J. Mater. Chem. A* **2014**, *2*, 6532–6539.

(48) Saxena, N.; Keilhofer, J.; Maurya, A. K.; Fortunato, G.; Overbeck, J.; Müller-Buschbaum, P. Facile Optimization of Thermoelectric Properties in PEDOT:PSS Thin Films through Acido-Base and Redox Dedoping Using Readily Available Salts. *ACS Appl. Energy Mater.* **2018**, *1*, 336–342.

(49) Xia, Y.; Ouyang, J. PEDOT:PSS Films with Significantly Enhanced Conductivities Induced by Preferential Solvation with Cosolvents and Their Application in Polymer Photovoltaic Cells. *J. Mater. Chem.* **2011**, *21*, 4927.

(50) Cho, H.; Cho, W.; Kim, Y.; Lee, J.; Kim, J. H. Influence of Residual Sodium Ions on the Structure and Properties of Poly(3,4-Ethylenedioxythiophene):Poly(Styrenesulfonate). *RSC Adv.* **2018**, *8*, 29044–29050.

(51) Pettersson, L. A. .; Ghosh, S.; Inganäs, O. Optical Anisotropy in Thin Films of Poly(3,4-Ethylenedioxythiophene)–Poly(4-Styrenesulfonate). *Org. Electron.* **2002**, *3*, 143–148.

(52) Brédas, J. L.; Wudl, F.; Heeger, A. J. Polarons and Bipolarons in Doped Polythiophene: A Theoretical Investigation. *Solid State Commun.* **1987**, *63*, 577–580.

(53) Horii, T.; Li, Y.; Mori, Y.; Okuzaki, H. Correlation between the Hierarchical Structure and Electrical Conductivity of PEDOT/PSS. *Polym. J.* **2015**, *47*, 695–699.

(54) Kim, N.; Kee, S.; Lee, S. H.; Lee, B. H.; Kahng, Y. H.; Jo, Y.-R.; Kim, B.-J.; Lee, K. Highly Conductive PEDOT:PSS Nanofibrils Induced by Solution-Processed Crystallization. *Adv. Mater.* **2014**, *26*, 2268–2272.

(55) Kim, N.; Lee, B. H.; Choi, D.; Kim, G.; Kim, H.; Kim, J.-R.; Lee, J.; Kahng, Y. H.; Lee, K. Role of Interchain Coupling in the Metallic State of Conducting Polymers. *Phys. Rev. Lett.* **2012**, *109*, 106405.

(56) Kee, S.; Kim, N.; Kim, B. S.; Park, S.; Jang, Y. H.; Lee, S. H.; Kim, J.; Kim, J.; Kwon, S.; Lee, K. Controlling Molecular Ordering in Aqueous Conducting Polymers Using Ionic Liquids. *Adv. Mater.* **2016**, *28*, 8625–8631.

(57) Tu, S.; Tian, T.; Lena Oechsle, A.; Yin, S.; Jiang, X.; Cao, W.; Li, N.; Scheel, M. A.; Reb, L. K.; Hou, S.; Bandarenka, A. S.; Schwartzkopf, M.; Roth, S. V.; Müller-

Buschbaum, P. Improvement of the Thermoelectric Properties of PEDOT:PSS Films via DMSO Addition and DMSO/Salt Post-Treatment Resolved from a Fundamental View. *Chem. Eng. J.* **2022**, *429*, 132295.

(58) Li, X.; Zou, R.; Liu, Z.; Mata, J.; Storer, B.; Chen, Y.; Qi, W.; Zhou, Z.; Zhang, P. Deciphering the Superior Thermoelectric Property of Post-Treatment-Free PEDOT:PSS/IL Hybrid by X-Ray and Neutron Scattering Characterization. *npj Flex. Electron.* **2022**, *6*, 6.

(59) Li, X.; Liu, Z.; Zhou, Z.; Gao, H.; Liang, G.; Rauber, D.; Kay, C. W. M.; Zhang, P. Effects of Cationic Species in Salts on the Electrical Conductivity of Doped PEDOT:PSS Films. *ACS Appl. Polym. Mater.* **2021**, *3*, 98–103.

(60) Nardes, A. M.; Kemerink, M.; Janssen, R. A. J.; Bastiaansen, J. A. M.; Kiggen, N. M. M.; Langeveld, B. M. W.; van Breemen, A. J. J. M.; de Kok, M. M. Microscopic Understanding of the Anisotropic Conductivity of PEDOT:PSS Thin Films. *Adv. Mater.* **2007**, *19*, 1196–1200.

(61) Lang, U.; Müller, E.; Naujoks, N.; Dual, J. Microscopical Investigations of PEDOT:PSS Thin Films. *Adv. Funct. Mater.* **2009**, *19*, 1215–1220.

(62) Marcus, Y. On Enthalpies of Hydration, Ionization Potentials, and the Softness of Ions. *Thermochim. Acta* **1986**, *104*, 389–394.

(63) R. Williams. *pKa Values in Water Compilation*. https://organicchemistrydata.org/hansreich/resources/pka/pka_data/pka-compilation-williams.pdf (accessed 2023-06-13).

(64) Wijeyasinghe, N.; Regoutz, A.; Eisner, F.; Du, T.; Tsetseris, L.; Lin, Y.-H.; Faber, H.; Pattanasattayavong, P.; Li, J.; Yan, F.; McLachlan, M. A.; Payne, D. J.; Heeney, M.; Anthopoulos, T. D. Copper(I) Thiocyanate (CuSCN) Hole-Transport Layers Processed

from Aqueous Precursor Solutions and Their Application in Thin-Film Transistors and Highly Efficient Organic and Organometal Halide Perovskite Solar Cells. *Adv. Funct. Mater.* **2017**, *27*, 1701818.

(65) Garcia-Belmonte, G.; Munar, A.; Barea, E. M.; Bisquert, J.; Ugarte, I.; Pacios, R. Charge Carrier Mobility and Lifetime of Organic Bulk Heterojunctions Analyzed by Impedance Spectroscopy. *Org. Electron.* **2008**, *9*, 847–851.

(66) Leever, B. J.; Bailey, C. A.; Marks, T. J.; Hersam, M. C.; Durstock, M. F. In Situ Characterization of Lifetime and Morphology in Operating Bulk Heterojunction Organic Photovoltaic Devices by Impedance Spectroscopy. *Adv. Energy Mater.* **2012**, *2*, 120–128.

(67) Murgatroyd, P. N. Theory of Space-Charge-Limited Current Enhanced by Frenkel Effect. *J. Phys. D. Appl. Phys.* **1970**, *3*, 308.

(68) Mihailetchi, V. D.; Xie, H. X.; de Boer, B.; Koster, L. J. A.; Blom, P. W. M. Charge Transport and Photocurrent Generation in Poly(3-Hexylthiophene):Methanofullerene Bulk-Heterojunction Solar Cells. *Adv. Funct. Mater.* **2006**, *16*, 699–708.